Geotech Geol Eng (2019) 37:13–23
https://doi.org/10.1007/s10706-018-0585-9

ORIGINAL PAPER

Numerical Simulation on Uniaxial Compression Failure of A Roof Rock–Coal–Floor Rock Composite Sample with Coal Persistent Joint

D. W. Yin · Xiangxi Meng

Received: 29 March 2018 / Accepted: 22 May 2018 / Published online: 26 May 2018

Abstract Geological dynamic hazards during coal mining can be induced by the structural instability of a composite structure of roof rock, coal and floor rock layers, whereas the joint in coal plays a vital role in the corresponding structural instability. In this paper, the effects of coal persistent joint on the uniaxial compression failure of a roof rock–coal–floor rock composite sample were analyzed using PFC^{2D} software. The results show that with an increase of included angle α between the loading direction and coal persistent joint plane, the uniaxial compressive stress (UCS) and peak strain of the composite sample decreased firstly and then increased. The change of elastic modulus was not obvious with α. The UCS and peak strain at α of 45° were the smallest. Additionally, the coal bodies in composite samples were mainly destructed as a shear failure. The roof or floor rock presented a tensile failure or no damage. And four failure patterns were observed for composite samples after failure, i.e., inverted V-shaped shear failure in coal and tensile failure in roof or floor rock, M-shaped shear failure in coal and tensile failure in floor rock, shear failure along the joint plane in coal and tensile failure in roof and floor rocks, shear failure along partial joint plane without obvious damage for roof or floor rock.

Keywords Geological dynamics hazards · Particle flow simulation · Roof rock–coal–floor rock (RR–C–FR) composite sample with coal persistent joint · Uniaxial compression failure · Strength characteristics

1 Introduction

Rock of underground coal mining is layered stratum formed by sedimentation. Therefore, the coal mining area is a combined structure composed of roof rock layer, coal seam and floor rock layer. The mechanical properties of combined structure play an important role in the coal safety production and coalminer's life safety. It is well known that the catastrophic instability and failure of a combined structure can induce the geological dynamic hazards, such as rock burst, coal and gas outburst (Huang and Liu 2013; Lu et al. 2015; Paul et al. 2012; Qin et al. 2006; Zhao et al. 2016; Petukhov and Linkov 1979; Yin et al. 2017; Chen et al. 2016). In the laboratory tests or numerical simulation tests, the different interbedded modes of coal and rock layers in coalmine were simplified as a composite sample composed of coal and rock with bonded (Paul et al. 2012; Zuo et al. 2016; Zhang et al. 2012) or freely overlapped into a whole body for studying the catastrophic instability and failure of a combined

D. W. Yin · X. Meng (✉)
State Key Laboratory of Mine Disaster Prevention and Control, Shandong University of Science and Technology, Qingdao 266590, China
e-mail: mxxsdust@126.com

structure (Zhao et al. 2008, 2014; Liu et al. 2015; Chen et al. 2017), including the roof rock–coal composite sample, coal–floor rock composite sample and roof rock–coal–floor rock composite sample, as shown in Fig. 1.

Through the laboratory tests and numerical simulation tests on the catastrophic instability and failure of composite samples, many interesting results were achieved. The effects of rock strength and homogeneity, height ratio of rock to coal, combination mode, interfacial angel, loading and unloading rate and confining pressure, etc., on the catastrophic instability and failure of the composite sample were studied and discussed (Huang and Liu 2013; Lu et al. 2015; Paul et al. 2012; Qin et al. 2006; Zhao et al. 2016; Petukhov and Linkov 1979; Zhao et al. 2008; Liu et al. 2015; Chen et al. 2017). Additionally, the interaction theory model for two rock masses was established and the interaction mechanisms were studied. And considering interface effect, the compression-shear strength criterion of a roof rock–coal composite model was established and analyzed by Zhao et al. (2014). The above studies are important to understand the catastrophic instability and failure of composite sample of coal and rock layers.

However, rock and coal are natural materials formed by the aggregation of mineral particles and cement with a determinate rule under the long-term geological effects. Compared with the rock, the raw coal is relatively soft and broken with a lot of initial defects, such as joints, fractures and various micro-inclusions and pores (Xu et al. 2013; Yin et al. 2017). And in the practical engineering, the coal's initial defects play an important role in the catastrophic instability and failure of the combined structure consisting of coal and rock layers (Lu et al. 2015). Unfortunately, there are few studies on the effects of coal's initial defects on the catastrophic instability and failure of the combined structure. Using PFC^{2D} software, Yin et al. (2017) studied and analyzed the effect of joint angle in coal on failure mechanical behavior of roof rock–coal composite sample.

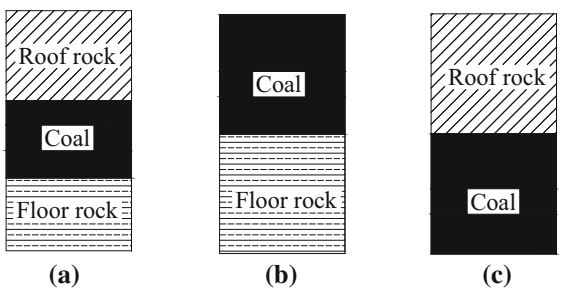

Fig. 1 Composite samples of coal and rock layers

The joint is a typical initial defect for coal (Cao et al. 2016; Xu et al. 2013; Liang et al. 2012). In this study, the uniaxial compression simulation tests on RR–C–FR composite samples with coal persistent joint were conducted using PFC^{2D} software and the effects of coal persistent joint on the uniaxial compression failure of RR–C–FR composite sample were studied and analyzed.

2 Numerical Model for RR–C–FR Composite Sample with Coal Persistent Joint

2.1 Particle Flow Code

The particle flow code (PFC) is an effective method to study the macro-mechanics problems of an analytic object (including construction, rock mass, etc.) at the micro-level (Yin et al. 2018). There are two bonding models in PFC^{2D} software, including the contact bond model and parallel bond model (Wang and Tian 2018). Among them, the parallel bond model refers to plane-to-plane bond and the moment of force can be transmitted, which can be applied to well simulate the compact material, such as rock and coal materials. Therefore, in this study, the uniaxial compression model for the RR–C–FR composite sample with coal persistent joint was built using the parallel bond.

2.2 Micro-parameters of Coal, Roof and Floor Rocks

Before simulating the uniaxial compression test of RR–C–FR composite samples with coal persistent joint, we must know the micro-parameters of coal and rock. However, these micro-parameters cannot be directly obtained by the laboratory tests. Firstly, a lot of numerical simulation tests with similar conditions as the laboratory tests, were carried out for determining these micro-parameters. And the micro-parameters determination is the process of minimizing the error between simulation and experimental results, which is achieved by adjusting the micro-parameters to match the elastic modulus, Poisson's ratio, peak

stress of standard rock or coal specimen (φ50 mm × 100 mm) provided by the laboratory test.

For convenience's sake, the micro-parameters of roof rock were taken same as that of the floor rock. And the micro-parameters for rock and coal provided by Zhao et al. (2016) and Yin et al. (2017) were used to conduct the simulation test, which are given in Table 1.

2.3 Numerical Model Construction

In this study, the coal, roof and floor rocks are freely overlapped into a whole body in natural contact and the contact surface is the bedding plane without the cohesive force. The uniaxial compression model for RR–C–FR composite sample with coal persistent joint was established and generated by radius extension, as shown in Fig. 2. The wall is lengthened appropriately for preventing the spill-out of the particles. The model size is 50 mm width × 100 mm height. And the heights of roof rock, coal and floor rock are 30, 40 and 30 mm, respectively. A total of 21,390 particles were generated in the model. The minimum particle radius is 0.2 mm, and the maximum particle radius is 0.3 mm. The origin of coal persistent joint is in the coal center. And the particles through the bedding planes are colored in red and the particles through the coal persistent joint plane are colored in blue.

Based on various numerical simulation tests on the jointed rock mass, the micro-parameters of bedding and joint planes were weakened and set as very small values (Kulatilake et al. 2001; Park and Song 2009; Huang and Yang 2015; Yin et al. 2017). In this study, the friction coefficients of bedding planes and coal persistent joint plane were set as 0.1, and their parallel bond normal strengths and parallel bond tangential strengths were all set as 0.

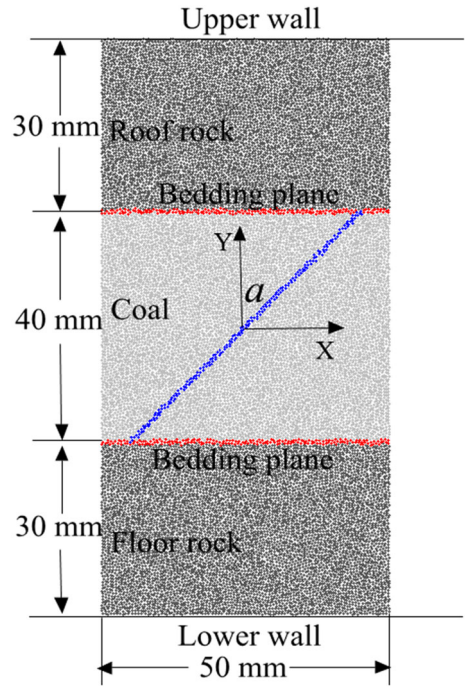

Fig. 2 Numerical model for RR–C–FR composite sample with coal persistent joint

2.4 Simulation Test Conditions

For studying the effects of coal persistent joint on the uniaxial compression failure of RR–C–FR composite sample, the included angle of α (Fig. 2) between the coal persistent joint plane and loading direction were taken as 0°, 15°, 30°, 45°, 60°, 75° and 90°,

Table 1 Micro-parameters of rock and coal Reproduced with permission from (Zhao et al. 2016; Yin et al. 2017)

Parameters	Roof and floor rocks	Coal	Parameters	Roof and floor rocks	Coal
Minimum particle size/mm	0.2		Parallel bond elastic modulus/GPa	12	4
Particle size ratio	1.5		Parallel bond normal strength/MPa	45	15
Density/(kg/m^3)	2600	1800	Parallel bond tangential strength/MPa	45	15
Contact modulus of the particle/GPa	12	4	Parallel bond normal stiffness/tangential stiffness	2.5	
Parallel bond radius multiplier	1		Normal stiffness/tangential stiffness	2.5	
Coefficient of friction			0.5		

respectively. And the loading is performed by moving the upper wall at a loading rate of 0.05 m/s.

3 Simulation Results Analysis

3.1 Effects of Coal Persistent Joint on Stress–Strain Behavior

Figure 3 shows the stress–strain curves of RR–C–FR composite samples with coal persistent joint. Table 2 shows the simulation results, including the UCS, peak strain and elastic moduli. Figure 4 presents the relationships between the UCS, peak strain and α.

In Fig. 3, the stress–strain curves of composite samples with coal persistent joint are similar to that of the intact composite sample, including the linear elastic deformation stage, non-linear deformation stage, post-peak strain softening and residual strength stage. In the linear elastic deformation stage, the stress–strain curves are basically coincident, illustrating that the elastic moduli are basically equal to that of the intact composite sample and changeless with the increase of α, which can also be verified in Table 2. The elastic modulus of composite sample is achieved by the slope of linear elastic deformation stage in stress–strain curve. In Table 2, the elastic modulus varies slightly with the increase of α and basically similar to that of the intact composite sample. And compared with the intact composite sample, the largest decrease of the elastic modulus of composite sample is 3.77% at α of 45°. The reason for this phenomenon is principally that there is no initial compression stage in PFC, which is different form the physical test (Yin et al. 2018).

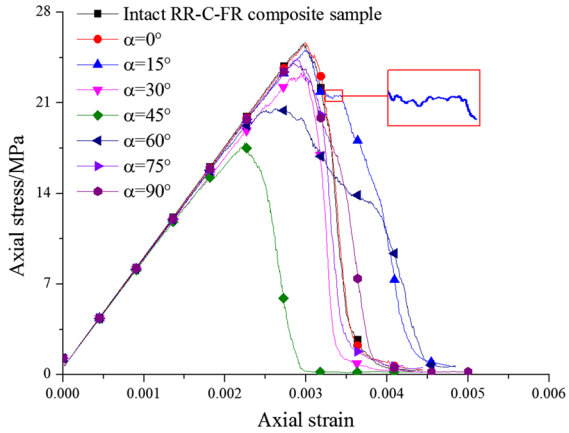

Fig. 3 Stress–strain curves of RR–C–FR composite samples with coal persistent joint

In Table 2 and Fig. 4, the coal persistent joint affects the UCS and peak strain of RR–C–FR composite sample. And with the increase of α, the UCS and peak strain decrease in the first place and then increase, agreeing with that of the UCS and peak strain of single jointed rock sample (Huang and Yang 2015). The UCS and peak strain of the composite sample at α of 45° are lowest, which are 17.912 MPa and 0.22448%, respectively. When α are 0°, 15°, 75° and 90°, the UCSs and peak strains are almost same as that of the intact composite sample, illustrating that the coal persistent joint within the above-mentioned range of α has little effects on UCS and peak strain. However, when α are 45° and 60°, compared with the intact composite sample, the UCSs decrease by 29.92 and 19.49%, respectively. And the corresponding peak strains decrease by 24.33 and 11.65%, respectively. It can been that the UCSs and peak strain are much less than that of the intact composite sample, indicating the coal persistent joint within the above-mentioned range of α has large effects on the UCS and peak strain of the composite sample. Additionally, the coal persistent joint has a large effect on the composite sample UCS at α of 30°, but a little effect on the peak strain. And compared with the intact composite sample, the UCS and peak strain decrease by 7.82 and 0.83%, respectively.

3.2 Effects of Coal Persistent Joint on Failure Pattern

Figure 5 gives the final failure patterns of RR–C–FR composite samples. When α is 0° or 75°, the failure of composite sample mainly occurs within coal and roof rock bodies, basically consistent with that of the intact composite sample. And the coal body has undergone an inverted V-shaped shear failure and tensile failure occurs in the roof rock body. And no obvious damage is observed for the floor rock. The coal body is broken into three parts and the roof rock is broken into two parts. Correspondingly, the fragmentation degrees of composite samples are relatively small, verified in Fig. 6. Figure 6 shows the micro-crack number of the composite samples after failure. In Fig. 6, the micro-crack number of composite samples at α of 0° and 75° are 2212 and 2034, respectively, close to that of the

Table 2 Numerical simulation results of the RR–C–FR composite samples under uniaxial compression

Category	UCS/MPa	Elastic modulus/GPa	Peak strain/%	Relationship of UCS between intact composite sample and composite sample with coal persistent joint	Relationship of elastic modulus between intact composite sample and composite sample with coal persistent joint	Relationship of peak strain between intact composite sample and composite sample with coal persistent joint
Intact composite sample	25.56	8.54	0.29664	–	–	–
$\alpha = 0°$	25.69	8.50	0.29928	Increase by 0.49%	Decrease by 0.53%	Increase by 0.89%
$\alpha = 15°$	25.07	8.40	0.29814	Decrease by 1.92%	Decrease by 1.66%	Increase by 0.51%
$\alpha = 30°$	23.33	8.22	0.29419	Decrease by 7.82%	Decrease by 3.77%	Decrease by 0.83%
$\alpha = 45°$	17.91	8.29	0.22448	Decrease by 9.92%	Decrease by 2.91%	Decrease by 4.33%
$\alpha = 60°$	20.58	8.40	0.26207	Decrease by 9.49%	Decrease by 1.71%	Decrease by 1.65%
$\alpha = 75°$	24.47	8.44	0.28924	Decrease by 4.28%	Decrease by 1.23%	Decrease by 2.49%
$\alpha = 90°$	24.07	8.44	0.28477	Decrease by 5.83%	Decrease by 1.17%	Decrease by 4.00%

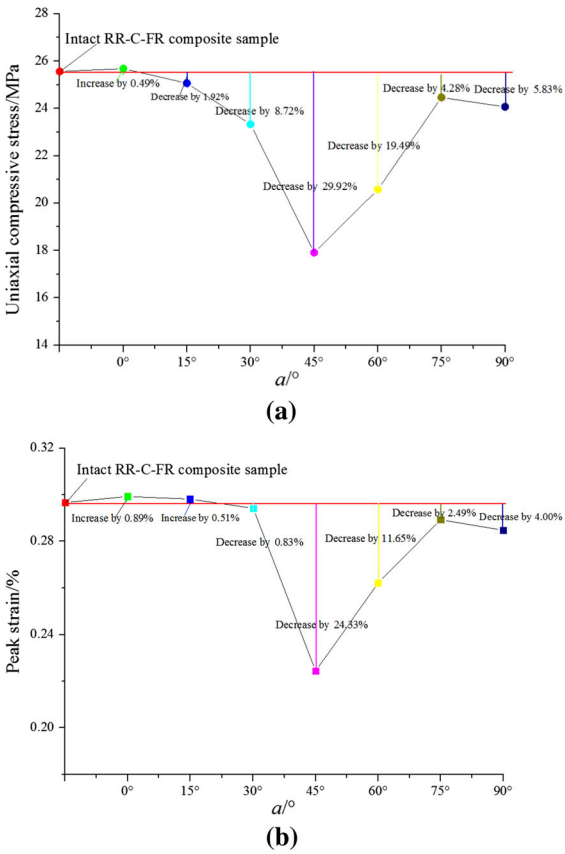

Fig. 4 Relationships between the UCS, peak strain and α. **a** Relationship between UCS and α, **b** Relationship between the peak strain and α

intact composite sample. However, when α is 15° or 90°, the failure mainly occurs within the coal and floor rock bodies. The coal bodies occur a V-shaped shear failure at α of 90° and a M-shaped shear failure at α of 15°. And the tensile failure is found in the floor rock body, no apparent damage is observed for roof rock. Moreover, the fragmentation degrees of composite samples are relatively large, especially at α of 15°. And compared with the intact composite sample, the micro-crack numbers increase by 47.16 and 18.52%, respectively. Additionally, the shear failure along the joint plane within the coal body and tensile failures within the roof and floor rocks bodies cause the catastrophic instability and failure of the composite sample at α of 30° and 45°. And the fragmentation degree is greatly reduced. After failure, there are 1722 and 975 micro-cracks, respectively, decreasing by 21.83 and 55.74% compared the intact composite sample. Meanwhile, the failure of composite sample at α of 60° is caused by the shear failure along partial joint plane within the coal body. And no apparent damage is found for roof and floor rocks. The shear failure zone width is large, the micro-crack number after failure increases by 15.25%, compared with the intact composite sample.

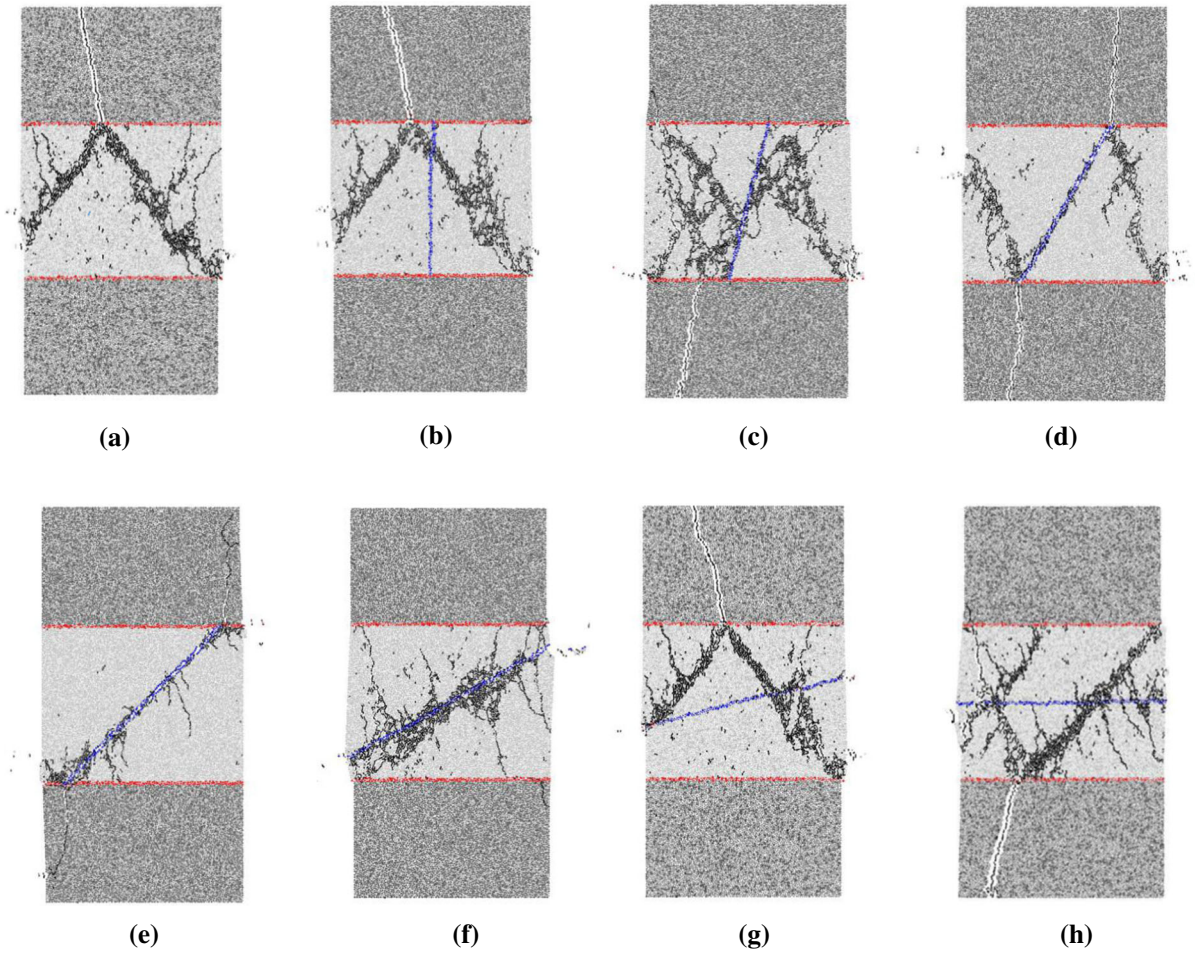

Fig. 5 Failure patterns of the RR–C–FR composite sample. **a** Intact composite sample, **b** $\alpha = 0°$, **c** $\alpha = 15°$, **d** $\alpha = 30°$, **e** $\alpha = 45°$, **f** $\alpha = 60°$, **g** $\alpha = 75°$, **h** $\alpha = 90°$

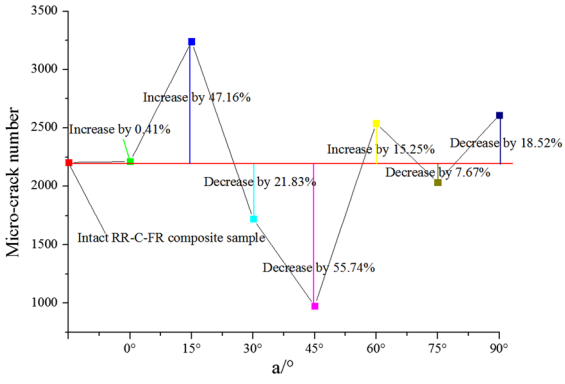

Fig. 6 Micro-crack numbers of RR–C–FR composite samples after failure

3.3 Micro-cracks Propagation and Coalescence of RR–C–FR Composite Sample

The propagation and coalescence of micro-cracks form the main control failure crack, causing the catastrophic instability and failure of RR–C–FR composite sample. Thus, the studies of micro-cracks propagation and coalescence are of great importances to understand the failure characteristics of composite sample with coal persistent joint. Figure 7 shows the micro-cracks propagation and coalescence in composite samples. Among them, the micro-cracks are represented as thick black lines.

In Fig. 7, at the initial stage of loading, the stress intensity transmitted between the particles is less than the bonding strength between particles, thus no micro-

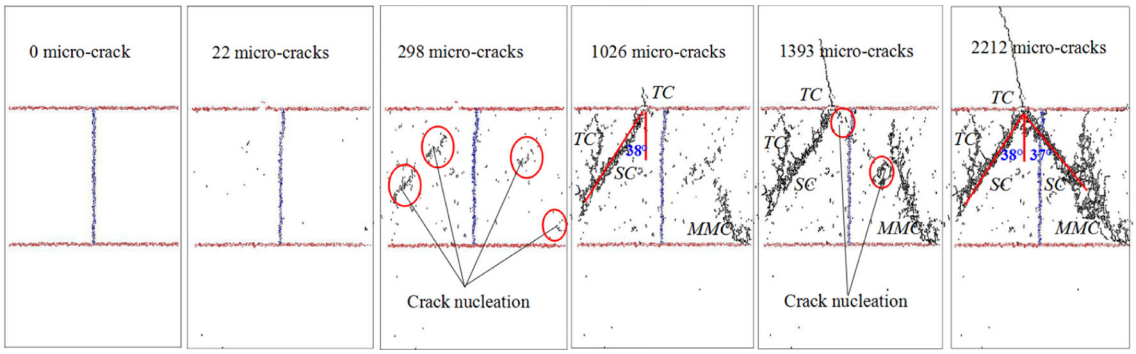

1: $\sigma = 0MPa$ 2: $\sigma = 20.55MPa$ 3: $\sigma = 25.685MPa$ (UCS) 4: $\sigma = 23.104MPa$ 5: $\sigma = 20.562MPa$ 6: Final failure

(a)

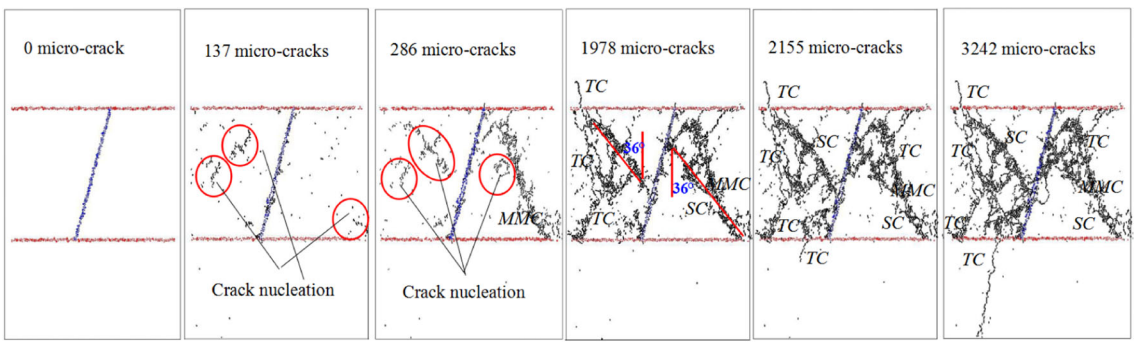

1: $\sigma = 0MPa$ 2: $\sigma = 23.516MPa$ 3: $\sigma = 25.069MPa$ (UCS) 4: $\sigma = 18.237MPa$ 5: $\sigma = 17.038MPa$ 6: Final failure

(b)

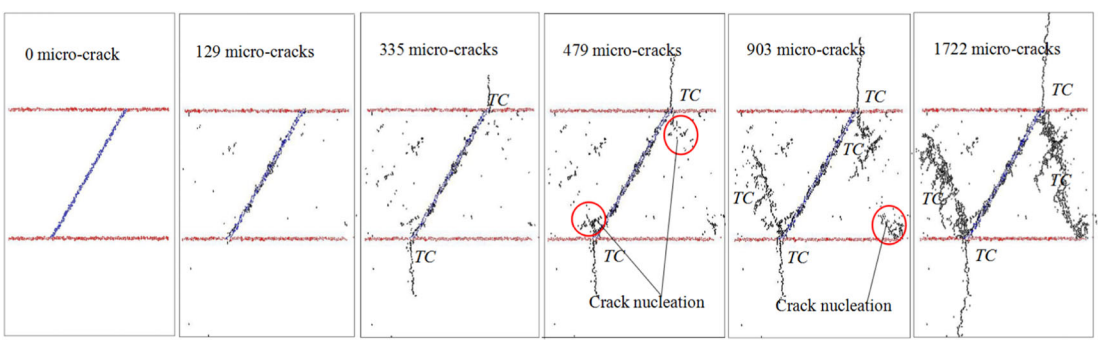

1: $\sigma = 0MPa$ 2: $\sigma = 21.181MPa$ 3: $\sigma = 23.333MPa$ (UCS) 4: $\sigma = 22.721MPa$ 5: $\sigma = 21.058MPa$ 6: Final failure

(c)

Fig. 7 Micro-cracks propagation and coalescence in RR–C–FR composite samples (*SC* shear crack, *TC* tensile crack, *MMC* mixed mode crack of shear and tensile cracks). **a** α = 0°, **b** α = 15°, **c** α = 30°, **d** α = 45°, **e** α = 60°, **f** α = 75°, **g** α = 90°

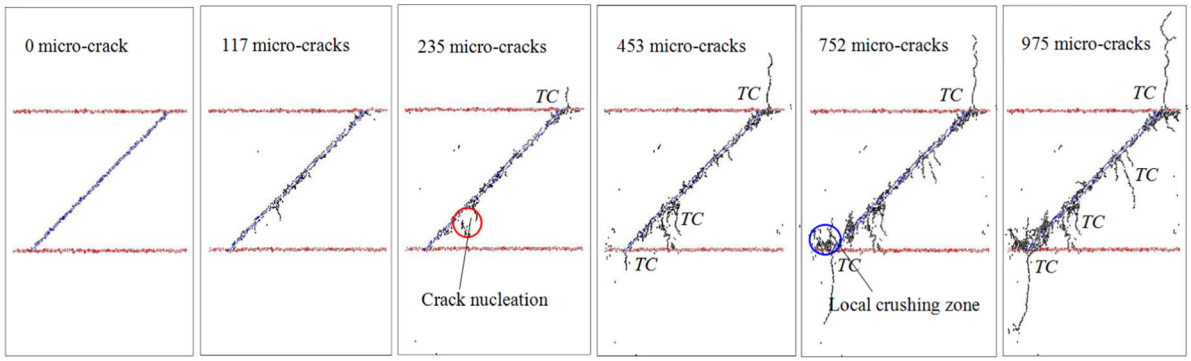

1: $\sigma = 0MPa$ 2: $\sigma = 16.008MPa$ 3: $\sigma = 17.912MPa$ (UCS) 4: $\sigma = 16.041MPa$ 5: $\sigma = 12.458MPa$ 6: Final failure

(d)

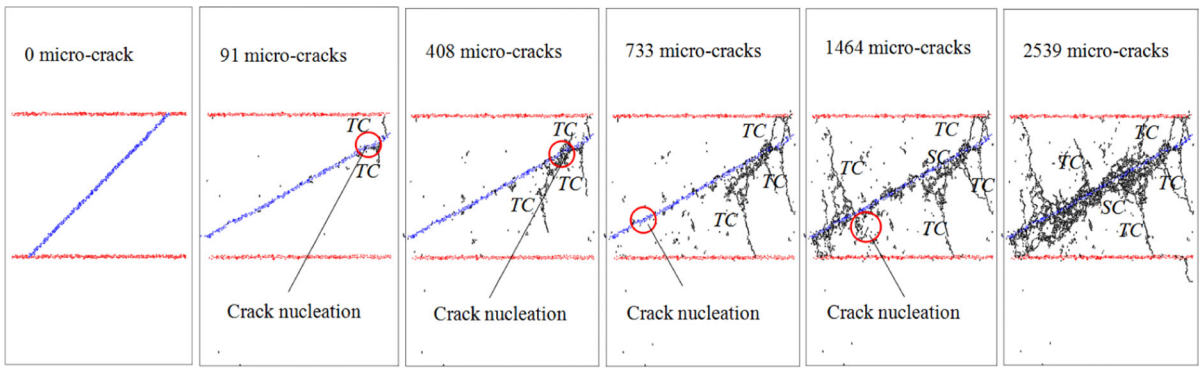

1: $\sigma = 0MPa$ 2: $\sigma = 19.057MPa$ 3: $\sigma = 20.578MPa$ (UCS) 4: $\sigma = 19.67MPa$ 5: $\sigma = 16.667MPa$ 6: Final failure

(e)

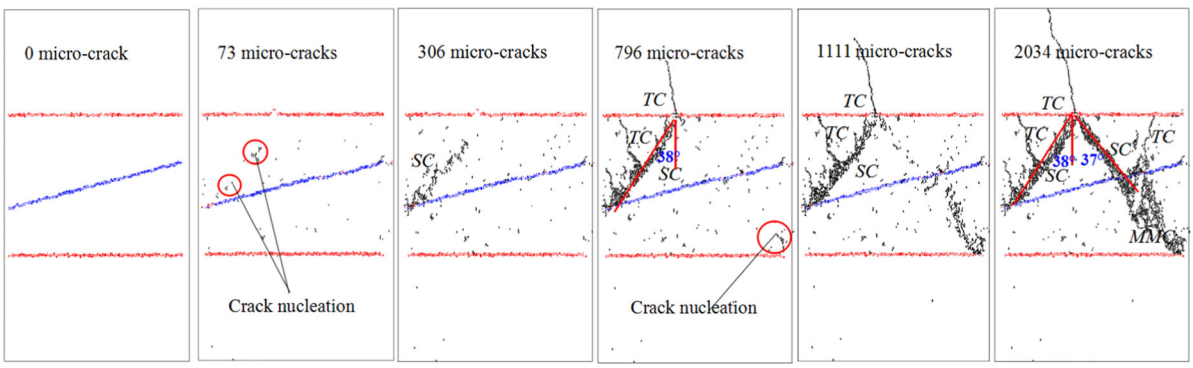

1: $\sigma = 0MPa$ 2: $\sigma = 22.649MPa$ 3: $\sigma = 24.466MPa$ (UCS) 4: $\sigma = 22.04MPa$ 5: $\sigma = 20.973MPa$ 6: Final failure

(f)

Fig. 7 continued

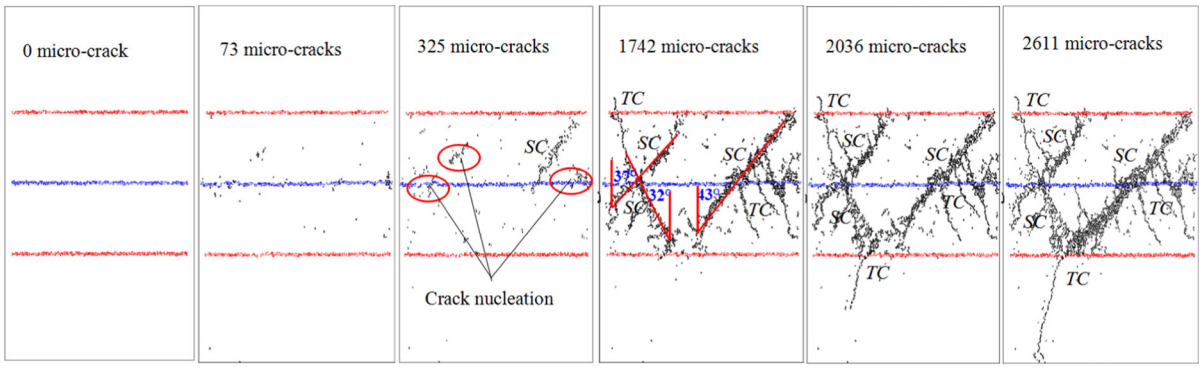

1: $\sigma = 0MPa$ 2: $\sigma = 21.107MPa$ 3: $\sigma = 24.07MPa$ (UCS) 4: $\sigma = 18.045MPa$ 5: $\sigma = 16.305MPa$ 6: Final failure

(g)

Fig. 7 continued

crack is generated. And with the increase of axial stress, when the stress intensity transmitted exceeds the bonding strength between particles, the micro-cracks will be generated. Moreover, micro-cracks are firstly randomly distributed within the coal body in composite samples at α of 0°, 15°, 75° and 90°. While, the micro-cracks are firstly distributed around the coal persistent joint at α between 30° and 60°. As the axial stress continues to increase, the micro-cracks propagation and coalescence of RR–C–FR composite sample with different α are characterized as follow:

(1) α of 0° and 75°

As the axial stress continues to increase, more micro-cracks are generated and they aggregate to form the crack nucleation within the coal body. With the further increase of axial stress, the micro-cracks in the crack nucleation propagate and coalesce upward at a certain angle and obvious macro-crack are formed, such as shear crack, tensile crack and mixed mode crack of shear and tensile cracks. In Fig. 7(a4) and (e4), a shear crack with an included angle of 38° between the shear crack plane and vertical direction, is observed in left upper part of coal body. And after extending to the upper bedding plane, the shear crack propagates as a tensile crack within the roof rock, illustrating that the shear crack tip stress intensity factor K_I exceeds the I-type crack fracture toughness K_{IC} of the roof rock. Also, a small tensile crack is found near the shear crack and its lower end is coincident to that of the shear crack. Meanwhile, a mixed mode crack of shear and tensile cracks is observed in right lower part of coal body at α of 0°. Additionally, the crack nucleation is formed in the right lower part of coal body at α of 75°.

In post-peak stage, the micro-cracks propagate and coalesce at a faster rate for forming the macro-failure crack of the composite sample. And the micro-cracks aggregate for forming the crack nucleation at the top tip of the shear crack and they propagate and coalesce downward in an included angle of 37° between the right shear crack plane and vertical direction for forming the right shear crack. Also, the micro-cracks in the crack nucleation in the right lower part of coal body at α of 75° propagate and coalesce upward for forming the mixed mode crack of shear and tensile cracks. Finally, in the residual deformation stage, the composite sample mainly slips along macro-failure plane for forming an inverted V-shaped shear failure in coal body and the roof rock body occurs the tensile failure.

2) α of 15° and 90°

The micro-cracks propagation and coalescence of composite samples at α of 15° and 90° are basically similar to that of composite samples at α of 0° and 75°. Firstly, the micro-cracks aggregate to form the crack nucleation within

the coal body. And then the micro-cracks propagate and coalesce at a certain angle for forming obvious macro-crack with the further increase of axial stress. Compared with composite samples at α of 0° and 75°, more obvious macro-cracks are generated in the composite samples at α of 15° and 90°, especially at α of 15°. And the shear crack propagate downward at a certain angle. Due to the shear crack tip stress intensity factor K_I exceeds the I-type crack fracture toughness K_{IC} of the floor rock, the shear crack propagates as a tensile crack within the roof rock when extending to the lower bedding plane. Finally, the coal bodies occur a V-shaped shear failure at α of 90° and a M-shaped shear failure at α of 15°. And the floor rock body occurs the tensile failure.

(3) α of 30° and 45°

As the axial stress continues to increase, two tips of the coal persistent joint firstly occur crack initiation and two tensile cracks are observed in the roof and floor rocks. In post-peak stage, the fast propagation and coalescence of tensile crack cause the floor and roof rocks failure. And the coal body occurs the slipping failure along the coal persistent joint plane at this stage. While, the micro-cracks aggregate to form the crack nucleation at the coal persistent joint tips at α of 30° and they propagate and coalesce to form the anti-wing tensile cracks within coal body, as shown in Fig. 7(c6). And the slipping failure along the coal persistent joint plane causes the local crushing zone near the lower tip of coal persistent joint at α of 45°, as shown in Fig. 7(d5).

(4) α of 60°

As the axial stress continues to increase, the upper tip of coal persistent joint occurs the crack initiation and two small tensile cracks are formed near the upper tip of coal persistent joint. And with the further increase of the axial stress, the micro-cracks aggregate for forming the crack nucleation near the upper tip of coal persistent joint and they propagate and coalesce downward at an included angle of 56° between the shear crack plane and vertical direction. And in post-peak stage, more micro-cracks are generated for forming other crack nucleation. And the micro-cracks propagate and coalesce for forming the shear failure along partial joint plane within the coal body, causing the catastrophic instability and failure of the composite sample.

4 Conclusions

The effects of the coal persistent joint on uniaxial compression failure of a RR–C–FR composite sample were studied using PFC^{2D} software. The main conclusions were drawn as below:

(1) The coal persistent joint affects the UCS and peak strain of RR–C–FR composite sample. With the increase of α, the UCS and peak strain decrease in the first place and then increase. And the UCS and peak strain at α of 45° are smallest. While, the change of elastic modulus is not obvious with α. The effects of coal persistent joint on the UCS and peak strain are relatively small at α of 0°, 15°, 75° and 90°, but a large effect at α of 45° and 60°. The coal persistent joint has a large effect on the UCS at α of 30°, but a little effect on the peak strain.

(2) The coal persistent joint affects the failure pattern of RR–C–FR composite sample. The coal bodies are all destructed as a shear failure. While, the roof or floor rock presents a tensile failure or no damage. Four typical failure patterns were observed for RR–C–FR composite samples with coal persistent joint, i.e., inverted V-shaped shear failure in coal and tensile failure in roof rock at α of 0° and 75°, V-shaped shear failure in coal and tensile failure in floor rock at α of 90°, M-shaped shear failure and tensile failure in floor rock at α of 15°, shear failure along the joint plane and tensile failure in roof and floor rocks at α of 30° and 45°, shear failure along partial joint plane without obvious damage for roof and floor rocks at α of 60°.

(3) Firstly, micro-cracks aggregate to form the crack nucleation within the coal body at α of 0°, 15°, 75° and 90°. And then the micro-cracks propagate and coalesce at a certain angle for forming macro-failure crack within the coal body. Generally, after propagating to the upper or lower bedding plane, the shear crack in coal body propagates as a tensile crack within the

roof or floor rock. While, the coal persistent joint tips at α of 30° and 45° firstly occur crack initiation and two tensile cracks are observed in roof and floor rocks. In post-peak stage, the propagation and coalescence of tensile crack cause the floor or roof rock failure. And the coal body occurs the slipping failure along the coal persistent joint plane. Additionally, the upper tip of coal persistent joint firstly occurs crack initiation at α of 60° and two small tensile crack are formed near the upper tip within the coal body. And the micro-cracks aggregate to form the crack nucleation near the upper tip of the coal persistent joint and they propagate and coalesce to cause shear failure of the composite sample.

Acknowledgements This study was supported by Graduate student science and technology innovation Project of Shandong University of Science and Technology (SDKDYC180201 and SDKDYC170308).

References

Cao RH, Cao P, Lin H, Pu CZ, Ou K (2016) Mechanical behavior of brittle rock-like specimens with pre-existing fissures under uniaxial loading: experimental studies and particle mechanics approach. Rock Mech Rock Eng 49(3):763–783

Chen SJ, Yin DW, Cao FW, Liu Y, Ren KQ (2016) An overview of integrated surface subsidence—reducing technology in mining areas of China. Nat Hazards 81(2):1129–1145

Chen SJ, Yin DW, Zhang BL, Ma HF (2017) Study on mechanical characteristics and progressive failure mechanism of roof-coal pillar structure body. Chin J Rock Mech Eng 36(7):1588–1598

Huang BX, Liu JW (2013) The effect of loading rate on the behavior of samples composed of coal and rock. Int J Rock Mech Min Sci 61:23–30

Huang YH, Yang SQ (2015) Discrete element study on strength and failure behavior of jointed sandstone with two sets of cross-joints. J China Coal Soc 40(S1):76–84

Kulatilake PHSW, Malama B, Wang J (2001) Physical and particle flow modeling of jointed rock block behavior under uniaxial loading. Int J Rock Mech Min Sci 38(5):641–657

Liang ZZ, Xing H, Wang SY, Williams DJ, Tang CA (2012) A three-dimensional numerical investigation of the fracture of rock specimens containing a pre-existing surface flaw. Comput Geotech 45:19–33

Liu J, Wang EY, Song DZ, Wang SH, Niu Y (2015) Effect of rock strength on failure mode and mechanical behavior of composite samples. Arab J Geosci 8(7):4527–4539

Lu CP, Liu GJ, Liu Y, Zhang N, Xue JH, Zhang L (2015) Microseismic multi-parameter characteristics of rockburst hazard induced by hard roof fall and high stress concentration. Int J Rock Mech Min Sci 76:18–32

Park JW, Song JJ (2009) Numerical simulation of a direct shear test on a rock joint using a bonded-particle model. Int J Rock Mech Min Sci 46(8):1315–1328

Paul A, Singh AP, John LP, Singh AK, Khandelwal M (2012) Validation of RMR-based support design using roof bolts by numerical modeling for underground coal mine of Monnet Ispat, Raigarh, India—A case study. Arab J Geosc 5(6):1435–1448

Petukhov IM, Linkov AM (1979) The theory of post-failure deformations and the problem of stability in rock mechanics. Int J Rock Mech Min Sci 16(2):57–76

Qin S, Jiao JJ, Tang CA, Li Z (2006) Instability leading to coal bumps and nonlinear evolutionary mechanisms for a coal pillar and roof system. Int J Solids Struct 43(25–26):7407–7423

Wang X, Tian LG (2018) Mechanical characteristics of coal–rock under different fracture-holes conditions: a numerical study based on particle flow code. Environ Earth Sci 77:297

Xu J, Cheng LC, Tan HY, Wang L, Wu H (2013) Effects of original cracks on macro-meso evolution law of coal shear failure. Chin J Rock Mech Eng 32(1):33–40

Yin DW, Chen SJ, Liu XQ, Ma HF (2017) Effect of joint angle in coal on failure mechanical behavior of roof rock–coal combined body. Q J Eng Geol Hydroge. https://doi.org/10.1144/qjegh2017-041

Yin DW, Chen SJ, Liu XQ, Ma HF (2018) Simulation study on strength and failure characteristics for granite with a set of cross-joints of different lengths. Adv Civ Eng 2018:1–10

Zhang ZT, Liu JF, Wang L, Yang HT, Zuo JP (2012) Effects of combination mode on mechanical properties and failure characteristics of the coal rock combinations. J China Coal Soc 37(10):1677–1681

Zhao YH, Jiang YD, Zhu J, Sun GZ (2008) Experimental study on precursory information of deformation of coal–rock composite sample before failure. Chin J Rock Mech Eng 27(2):339–346

Zhao ZH, Wang WM, Dai CQ, Yan JX (2014) Failure characteristics of three-body model composed of rock and coal with different strength and stiffness. Trans Nonferr Metal Soc 24(5):1538–1546

Zhao TB, Guo WY, Lu CP, Zhao GM (2016) Failure characteristics of combined coal–rock with different interfacial angles. Geomech Eng 11(3):345–359

Zuo JP, Chen Y, Zhang JW, Wang JT, Sun YJ, Jiang GH (2016) Failure behavior and strength characteristics of coal–rock combined body under different confining pressures. J China Coal Soc 41(11):2706–2713